Seventh International Conference on Computational Fluid Dynamics (ICCFD7), Big Island, Hawaii, July 9-13, 2012

ICCFD7-2403

Adjoint-based Optimization of the Flapping Wing Performance

M. Jones* and N. Yamaleev*
Corresponding author: nkyamale@ncat.edu

*North Carolina A&T State University, USA

Abstract: A time-dependent adjoint-based methodology developed in [AIAA 2008-5857 and AIAA J. Vol.48, No.6, pp.1195-1206, 2010] is used for optimization of the 3-D unsteady turbulent flow near a flapping wing. The sensitivities of the thrust coefficient to wing kinematic parameters are computed using the time-dependent discrete adjoint formulation. The unsteady discrete adjoint equations required for calculation of the sensitivity derivatives are integrated backward in time. The gradient of the objective functional computed using the adjoint formulation is then used to update the values of the kinematic design variables. The efficiency of this time-dependent optimization methodology is demonstrated by maximizing the performance of a wing undergoing insect-based flapping motion. Our numerical results show that the wing thrust coefficient and propulsive efficiency have been significantly increased after the optimization.

Keywords: Unsteady adjoint equations, Lagrange multipliers, time-dependent optimization, flapping wing, unsteady RANS equations.

1 Introduction

Insects and small birds represent fully functional examples of efficient small-scale flying devices. However, copying of wing kinematics and shape of flying animals is far form being sufficient to design and build effective, highly maneuverable, agile micro air vehicles (MAVs). Indeed, the current state-of-the-art materials, micro-scale actuators, propulsion systems, and power sources are different and in most cases less efficient than those created by Mother Nature over millions years of evolution. This lack in efficiency of currently available MAV components indicates that a different region of the design space as compared with that of flying insects and animals should be explored to be able to maximize the performance of flapping-wing microsystems. Therefore, designs inspired by flying animals can be used only as a preliminary conceptual design that requires further optimization for constructing efficient and agile flying micro-scale platforms optimized for size, weight, speed, and maneuverability. This is a very challenging optimization problem that involves hundreds or even thousands kinematics and shape design variables and is governed by highly unsteady vortex-dominated turbulent flows. Therefore, efficient, mathematically rigorous optimization techniques based on optimal control theory should be used for solving this class of problems.

In spite of significant progress in modeling and computational fluid dynamics (CFD) analysis of flapping- and rotary-wing platforms [1-5], questions related to optimal design of efficient micro air vehicles (MAV) have not yet been properly addressed especially in three dimensions because of the physics complexity and computational cost involved. Various parametric and sensitivity studies (e.g., see [1]) have revealed that there is an essentially nonlinear relationship between the major wing kinematic parameters (amplitude, frequency, phase shift angle), shape parameters (wing thickness, planform, twist, and camber), and global flow parameters (the Reynolds, Strouhal, and Mach numbers). Conventional parametric studies, which estimate the sensitivity to each individual design variable independently, do not take into account this nonlinear relationship between the main

parameters determining the MAV performance. Furthermore, parametric studies are extremely computationally expensive because of the very large dimensionality of the design space and therefore impractical for optimization and design of efficient flapping-wing microsystems.

Several attempts have recently been made to use genetic algorithms based on low-fidelity models [6], high-fidelity models [7], and experimental apparatus [8] for optimization of flapping-wing flows. Since these stochastic optimization techniques require thousands of evaluations of the objective functional for each design variable, all these approaches have been limited to optimization of 2-D flows with a very small number (less than 4) of design variables. Gradient-based methods provide a powerful alternative for optimization of flapping airfoils and wings. Culbreth et al. [9] uses a finite difference method coupled with a 3-D Navier-Stokes solver to evaluate the sensitivities of a modified propulsive efficiency to 4 spanwise twist design variables. In [10], a forward mode differentiation method governed by a 2-D Navier-Stokes solver has been successfully used to maximize thrust and propulsive efficiency of a pitching and plunging airfoil.

Unlike the forward mode differentiation methods which suffer from excessive cost caused by the need to solve the unsteady Navier-Stokes equations as many times as the number of design variables, an adjoint method provides the sensitivities at a cost which is comparable to that of a single flow solution and independent of the number of design variables. Adjoint-based optimization of flapping wing flows has been very rare and received significantly less attention [11, 12]. In the present paper the adjoint based methodology developed in [13, 14] is used to optimize the performance of an isolated wing undergoing insect-based flapping motion. Wing kinematic parameters, such as stroke and pitch angle amplitudes and frequencies, phase shift angle between pitching and flapping motions, the coordinates of a point with respect to which the stroke and pitch motions occur, are used as design variable. Our numerical results show that the wing performance significantly increases while all the imposed constraints are satisfied in the course of optimization, thus indicating that the developed methodology can be efficiently used for optimization and design of MAV systems.

2 Governing Equations and Numerical Method

The fully turbulent compressible flow near a wing undergoing an insect-based flapping motion is simulated using the 3-D unsteady Reynolds-Averaged Navier-Stokes (URANS) equations written in the integral conservation law form as follows:

$$\frac{\partial (V\mathbf{Q})}{\partial t} + \oint_{\Gamma} (\mathbf{F}_i - \mathbf{F}_v) \cdot \mathbf{n} dS = \mathbf{0}, \tag{1}$$

where V is a moving control volume bounded by the surface Γ, $\mathbf{Q}$ represents a vector of the volume-averaged conservative variables, $\mathbf{n}$ is the outward unit face normal vector, and $\mathbf{F}_i$ and $\mathbf{F}_v$ are the inviscid and viscous flux vectors, respectively. Note that for a moving control volume, the inviscid flux vector must account for the difference in the fluxes due to the movement of control volume faces. Given a flux vector $\mathbf{F}$ on a static grid, the corresponding flux vector $\mathbf{F}_i$ on a moving grid is defined as $\mathbf{F}_i = \mathbf{F}\text{-}\mathbf{Q}(\mathbf{W}\cdot\mathbf{n})$, where $\mathbf{W}$ is a local face velocity.

The governing equations are closed with the perfect gas equation of state and the Spalart-Allmaras turbulence model for the eddy viscosity. Note that for the special case of $\mathbf{Q}=const$, the conservation equations (1) reduce to the Geometric Conservation Law (GCL):

$$\frac{\partial V}{\partial t} + \oint_{\Gamma} \mathbf{W} \cdot \mathbf{n} dS = \mathbf{0}. \tag{2}$$

The GCL provides a precise relation between the rate of change of the time-dependent control volume and its local face velocity **W.** Though the GCL equation is a direct consequence of the governing equations (1) and is satisfied at the differential level, this is usually not the case at the discrete level. To preserve a constant solution on dynamic grids, the discrete GCL residual R_{GCL} is added to the discretized flow equations (see [15] for further details).

In the present study, the time derivative and contour integral in (1) are discretized using a 2nd-order backward difference (BDF2) formula and 2nd-order node-centered finite volume scheme [16],

respectively. The inviscid fluxes at cell interfaces are computed using Roe's approximate Riemann solver, and the viscous fluxes are approximated by a method equivalent to a 2nd-order finite element Galerkin procedure. The mesh velocity terms are evaluated with the BDF2 formula consistent with the discretization of the time derivative. An approximate solution of the linear system of equations formed within each time step is obtained with a multicolor Gauss-Seidel point-iterative scheme. The turbulence model is integrated all the way to the wall without the use of wall functions and is solved separately from the mean flow equations. The solver demonstrates high parallel scalability which is achieved through domain decomposition and message passing communication. The numerical method described above was implemented in a fully unstructured Reynolds-averaged Navier-Stokes solver called FUN3D [17], which has been used in all numerical studies presented in this paper.

3 Rigidly Moving Grid

To accurately resolve the flow near a wing during the entire flapping motion, a body-fitted mesh is regenerated at each time step, so that it moves rigidly along with the wing. The rigid mesh motion is generated by a 4x4 transformation matrix [15]. The transformation matrix enables general translations and rotations of the grid according to the following relation:

$$\mathbf{x} = T\mathbf{x}_0,$$

which moves a point from an initial position (x_0, y_0, z_0) to its new position (x, y ,z):

$$\begin{bmatrix} x \\ y \\ z \\ 1 \end{bmatrix} = \begin{bmatrix} r_{11} & r_{12} & r_{13} & t_x \\ r_{21} & r_{22} & r_{23} & t_y \\ r_{31} & r_{32} & r_{33} & t_z \\ 0 & 0 & 0 & 1 \end{bmatrix} \begin{bmatrix} x_0 \\ y_0 \\ z_0 \\ 1 \end{bmatrix}. \tag{3}$$

In Eq. (3), the 3x3 matrix R defines a general rotation, and the vector $\mathbf{t} = [t_x, t_y, t_z]^T$ specifies a translation. Note that the matrix T depends on time. One key feature of this approach is that multiple transformations telescope via matrix multiplication. This formulation is particularly attractive for composite parent-child body motion. Herein, the rotation associated with the wing pitching is specified relative to the stroke motion. For a rigid motion, the grid equation at time level n is defined as follows:

$$\mathbf{G}\left(\mathbf{X}^0, \mathbf{X}^n, \mathbf{D}\right) = \mathcal{R}\mathbf{X}^0 + \boldsymbol{\tau} - \mathbf{X}^n, \tag{4}$$

where $\boldsymbol{X}^0$ and $\boldsymbol{X}^n$ are the grid vectors at the initial and n-th time levels, $\mathcal{R}$ is a block-diagonal matrix.

4 Wing Kinematics

In the present analysis, the kinematics of an idealized insect wing motion is defined by specifying the following three angles associated with the stroke position θ, pitch angle α, and stroke deviation from the mean stroke plane, φ:

$$\begin{cases} \theta = \theta_0 \sin(2\pi f_{s0} t) + \theta_1[1 - \cos(2\pi f_{s1} t)] \\ \alpha = \alpha_0 \sin\left(2\pi f_{p0} t\right) + \alpha_1\left[1 - \cos\left(2\pi f_{p1} t\right)\right] \\ \varphi = \varphi_0 \sin(2\pi f_{d0} t) + \varphi_1[1 - \cos(2\pi f_{d1} t)] \end{cases} \tag{5}$$

where f_s, f_p, f_d are stroke, pitch, and deviation frequencies. These three angles are used to construct the corresponding rotation matrices of the form given by Eq. (3). These matrices are then multiplied together to form the final rotation matrix used to specify the current wing position.

The rotation associated with the stroke motion occurs with respect to the wing root. The wing flips (pitches) about an axis located approximately at 50% of the chord. For the baseline configuration, the pitching axis remains in the stroke plane throughout the entire motion, and the forward and backward stroke arcs are kinematically symmetric. Note that for this wing motion, the midpoint of the flip occurs precisely at the end of the forward stroke or the end of the backward stroke. The amplitudes and frequencies in Eq. (5) as well as the components of the center of rotation with respect of which the stroke, pitch, and deviation motions occur are used as design variables and optimized to maximize the thrust coefficient of the flapping wing.

5 Adjoint-based Time-Dependent Optimization Methodology

To increase the wing performance, the thrust coefficient is considered as a functional which is maximized by using optimal control theory, thus leading to the following discrete PDE-constrained optimization problem:

$$\begin{cases} \min F_{\text{obj}}(\boldsymbol{D}), \qquad F_{\text{obj}}(\boldsymbol{D}) = \sum_{n=N_b}^{N_e} f^n \Delta t,\ f^n = \left(C^n - C^n_{\text{target}}\right)^2 \\ \text{subject to: } V^n \dfrac{3\boldsymbol{Q}^n - 4\boldsymbol{Q}^{n-1} + \boldsymbol{Q}^{n-2}}{2\Delta t} + \boldsymbol{R}^n + \boldsymbol{R}^n_{GCL}\boldsymbol{Q}^{n-1} = 0 \\ \boldsymbol{G^n}(\boldsymbol{X}^0, \boldsymbol{X}^n, \boldsymbol{D}) = 0 \end{cases} \tag{6}$$

where $\boldsymbol{D}$ is a vector of the design variables, $\boldsymbol{Q^n}$ is a vector of conservative variables, C^n is an aerodynamic coefficient such as thrust, lift, drag, or their combination and C^n_{target} is its target value, N_b and N_e are time levels corresponding to a time interval over which the objective functional is minimized, $\boldsymbol{R}^n$ and $\boldsymbol{G^n}$ are the flow and grid residuals, and $\boldsymbol{R}^n_{GCL}$ is the geometric conservation law term.

The discrete time-dependent optimization problem (6) is solved by the method of Lagrange multipliers which is used to enforce the flow and grid equations (1, 4) as constraints. The Lagrangian functional is defined as follows:

$$L(\boldsymbol{D}, \boldsymbol{Q}, \boldsymbol{X}, \boldsymbol{\Lambda}_{\text{f}}, \boldsymbol{\Lambda}_{\text{g}}) = \sum_{n=1}^{N} f^n \Delta t + \sum_{n=1}^{N} [\boldsymbol{\Lambda}^{\boldsymbol{n}}_{\text{f}}]^{\text{T}} \left(V^n \frac{3\boldsymbol{Q}^n - 4\boldsymbol{Q}^{n-1} + \boldsymbol{Q}^{n-2}}{2\Delta t} + \boldsymbol{R}^n + \boldsymbol{R}^n_{GCL}\boldsymbol{Q}^{n-1} \right) \Delta t + \sum_{n=1}^{N} \left[\boldsymbol{\Lambda}^{\boldsymbol{n}}_{\text{g}}\right]^{\text{T}} \boldsymbol{G^n} \boldsymbol{\Delta t} \tag{7}$$

where $\boldsymbol{\Lambda}^{\boldsymbol{n}}_{\text{f}}$ and $\boldsymbol{\Lambda}^{\boldsymbol{n}}_{\text{g}}$ are vectors of Lagrange multipliers associated with the flow and grid equations, respectively, $\boldsymbol{D}$ is a vector of design variables, and $f^n = 0$ for $n < N_b$ and $n > N_e$. Note that terms corresponding to the initial conditions are omitted in Eq. (7).

Differentiating the Lagrangian with respect to $\boldsymbol{D}$, collecting the coefficients of $\partial \boldsymbol{Q}^n / \partial \boldsymbol{D}$, and setting them equal to zero, the following equations for the flow adjoint variables $\boldsymbol{\Lambda}_f$ are derived:

$$\frac{3V^n \boldsymbol{\Lambda}_f^n - 4V^{n+1}\boldsymbol{\Lambda}_f^{n+1}{}^{n+1} + V^{n+2}\boldsymbol{\Lambda}_f^{n+2}}{2\Delta t} + \left[\frac{\partial \boldsymbol{R}^n}{\partial \boldsymbol{Q}^n}\right]^T \boldsymbol{\Lambda}_f^n + \boldsymbol{R}^n_{GCL}\boldsymbol{\Lambda}_f^{n+1} = -\left[\frac{\partial f^n}{\partial \boldsymbol{Q}^n}\right]^T \tag{8}$$

The grid adjoint equations are obtained in a similar way (see [14] for details). The key advantage of the adjoint formulation is that the adjoint equations (8) are independent of the vector $\boldsymbol{D}$, and should be solved once at each optimization iteration, regardless of the number of the design variables. Since the first term in Eq. (8) approximates the negative time derivative, the unsteady adjoint equations have to be integrated backward in time. Therefore, the entire flow solution history should be available during the backward-in-time integration of the flow adjoint equations. In the present approach, the conservative variables, grid coordinates, and grid velocities are stored to disk at the end of each time step of the flow solution. During the integration of Eq. (8) in reverse time, the stored data is loaded

from disk. With the adjoint variables satisfying the flow and grid adjoint equations, the gradient of the Lagrangian with respect to $\boldsymbol{D}$ is calculated as follows:

$$\frac{dL}{d\boldsymbol{D}} = \sum_{n=1}^{N} \left(\frac{\partial f^n}{\partial \boldsymbol{D}} + \left[\boldsymbol{\Lambda}_f^n\right]^T \left(\frac{\partial \boldsymbol{R}^n}{\partial \boldsymbol{D}} + \frac{\partial \boldsymbol{R}_{GCL}^n}{\partial \boldsymbol{D}} \boldsymbol{Q}^{n-1} \right) + \left[\boldsymbol{\Lambda}_g^n\right]^T \frac{\partial \boldsymbol{G}^n}{\partial \boldsymbol{D}} \right) \Delta t \qquad (9)$$

As in Eq. (7), terms corresponding to the initial conditions are omitted. A minimum of the objective functional is found by using a gradient-based optimization package PORT [18].

6 Numerical Results

The adjoint-based optimization methodology described above is used to improve the performance of an isolated wing undergoing insect-based flapping motion. We consider a rigid wing whose shape resembles a wing profile of the fruit fly, *Drosophila melanogaster*. The hovering wing is assumed to be operating in quiescent conditions. The wing has the semi-circular leading and trailing edges, a mean aspect ratio of 2.24, and a thickness-to-chord ratio of 0.04. The baseline Reynolds and Mach numbers based on the wing maximum tip speed are set equal to 4,800 and 0.06, respectively.

The baseline kinematic motion consists of two rotations, each occurring at the reduced frequency of 0.262. The first rotation is a stroke motion with amplitude of 60^0. The second rotation is a pitch motion with amplitude of 45^0. The amplitudes and frequencies of the stroke and pitch motions, as well as the coordinates of the center of rotation are used as design variables. Thus, there are a total of 15 design variables for each test problem considered.

We consider two test problems. For the first problem, the objective functional is given by Eq. (6), where the aerodynamic coefficient C is the wing thrust and N_b =41 and N_e = 80 that correspond to the second full stroke of the baseline configuration. The thrust target value is set to be 10, which is significantly higher than its baseline value. Figure 1 shows the convergence history of the objective functional. The objective functional has been reduced from its initial value of 18,115 to a final value of 12,991 over 20 design cycles. Note that the major reduction occurs during the first 6 design cycles after which further improvements are negligible. The stroke and pitch angle profiles before and

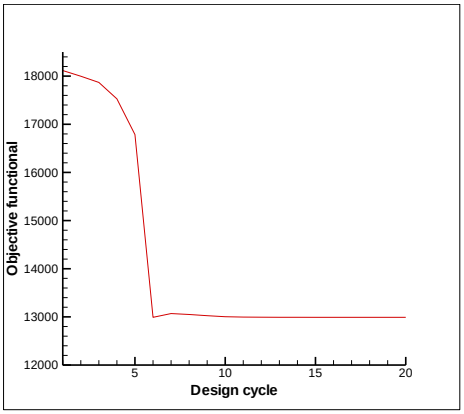

Figure 1: Convergence history of the objective functional for the 1st test problem.

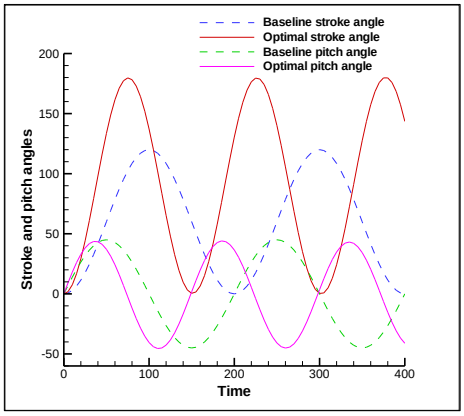

Figure 2: Baseline and optimal stoke and pitch angle profiles.

after the optimization are presented in Fig. 2. The stoke amplitude has been significantly increased during the optimization, reaching its upper bound value of 90^0, while the pitch angle amplitude remains nearly the same. The deviation from the mean stroke plane has not been appreciably changed and is therefore not presented in Fig. 2. The optimizer has increased not only the stroke amplitude, but also its frequency, such that three peaks now occur within the same time interval used to define the objective functional.

A detailed comparison of the baseline and optimal solutions is presented in Fig.3 showing snapshots of an iso-surface of the q-criterion colored with pressure contours at three time levels n = 48, 55, 63. As one can see in Fig. 3, the optimization of wing kinematics significantly strengthens the

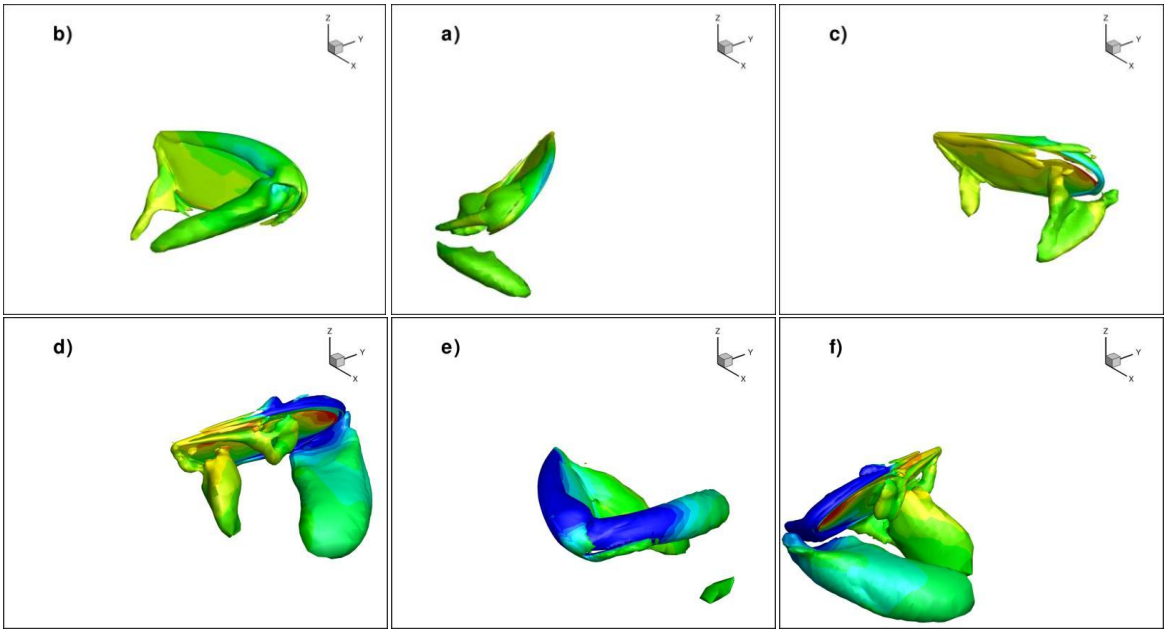

Figure 3: Iso-surface of the q-criterion colored with pressure contours at n = 48, 55, 63, obtained with the baseline (top row) and optimized (bottom row) wing kinematics.

leading edge and root vortices, thus considerably reducing the pressure in the upper surface of the wing and increasing the thrust.

The baseline and optimized thrust profiles are shown in Fig. 4. The mean value of the thrust coefficient has been increased by a factor of 5.5 as compared with its baseline value. Note, however, that the increase in the stroke and pitch frequencies has also resulted in increase in the drag coefficient, as one can see in Fig. 5 presenting a thrust-to-drag ratio before and after the optimization. The thrust-to-drag ratio can also be interpreted as a modified propulsive efficiency. As follows from this comparison, the stroke-averaged propulsive efficiency of the optimized configuration is very similar to that obtained with the baseline wing kinematics. It is not surprising because the objective of this optimization problem is to maximize the thrust coefficient generated by the wing rather than its

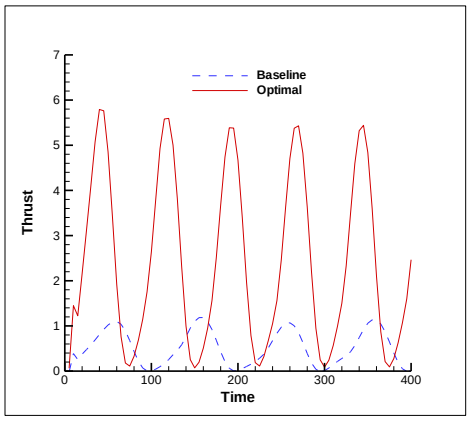

Figure 4: Baseline and optimal thrust profiles

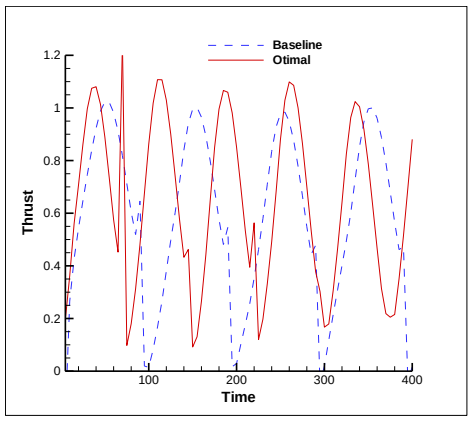

Figure 5: Propulsive efficiency before and after optimization for the 1st test problem.

propulsive efficiency.

As has been mention above, maximization of the thrust coefficient also increases the drag, thus indicating that significantly higher power is required for operating the optimized flapping wing as compared with the baseline configuration. To overcome this problem, the objective functional in the second test problem has been penalized as follows:

$$f^n = \left(C_z^n - C_{\text{target}}^n\right)^2 + \omega_1 (C_x^n)^2 + \omega_2 \left(C_y^n\right)^2 \qquad (10)$$

where ω_1 and ω_2 are weight coefficients which are both set to be 5. Note that the target thrust value is equal to that used in the previous test case, which is significantly higher that its baseline value. The last two terms in Eq. (10) penalize the objective functional in such a way that the functional rapidly increases if both C_x and C_y deviate from zero, thus minimizing the x- and y-components of the aerodynamic force.

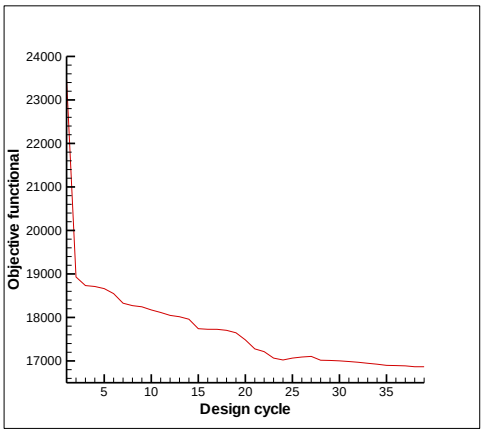

Figure 6: Convergence history of the objective functional for the 2nd test case.

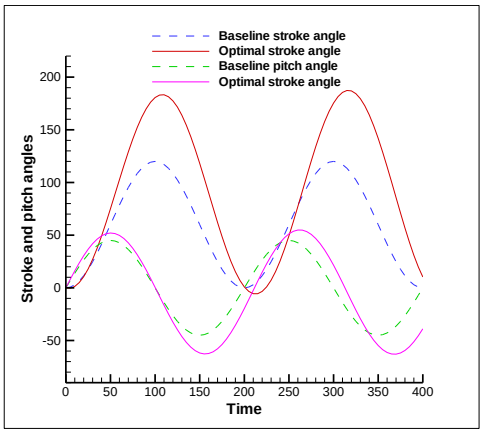

Figure 7: Baseline and optimal stoke and pitch angle profiles.

The convergence history of the objective functional given by Eq. (10) is presented in Fig. 6. The value of the objective functional rapidly drops from 23,500 to 19,000 over the first design cycle, after which it keeps steadily decreasing until it reaches its lowest value of 16,990. For this test case, the optimizer performed 40 flow solutions and 24 adjoint solutions. In contrast to the previous test case, the stroke and pitch frequencies providing the optimal wing performance are practically equal to those of the baseline configuration, as evident in Fig. 7. The main reason why the optimal values of the stroke and pitch cycle frequencies have not been appreciably changed during the optimization is the presence of the penalty terms in the objective functional given by Eq. (10). A conclusion that can be drawn from this observation is that significant increase in the wing flapping frequency does not necessarily improve the wing propulsive efficiency. Another key distinction of this optimal solution as compared

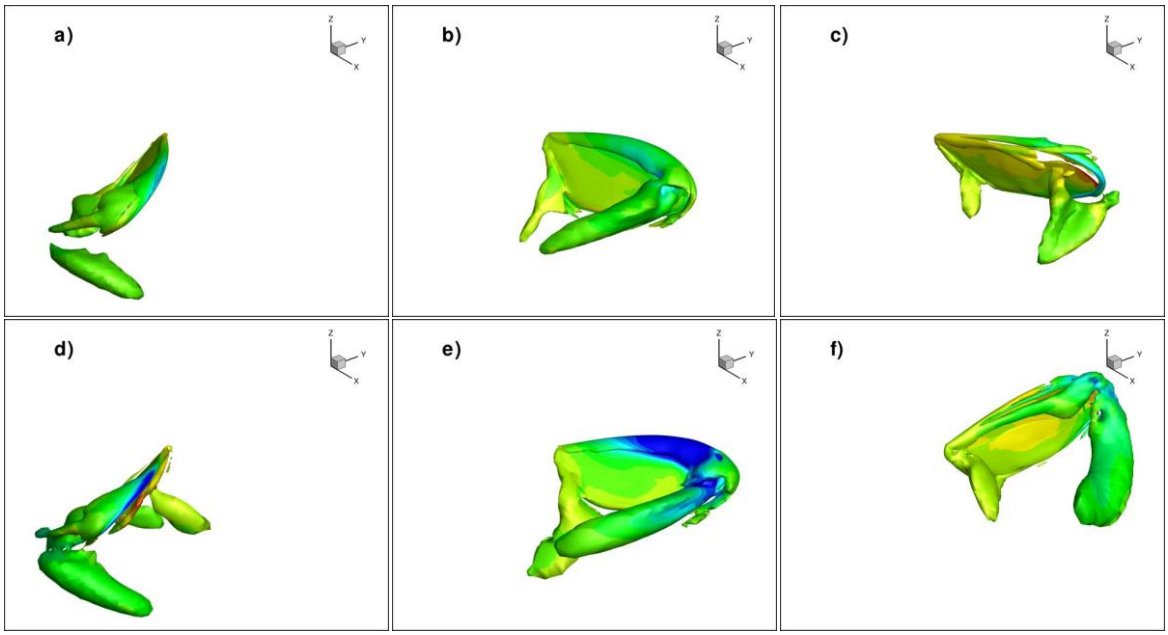

Figure 8: Iso-surface of the q-criterion colored with pressure contours at n = 48, 55, 63, obtained with the baseline (top row) and optimized (bottom row) wing kinematics.

with the one obtained in the previous test case is that the pitch angle amplitude reaches its upper bound value of 55^0. Note that the stroke angle amplitude also attains its upper bound value of 90^0. The final values of the other design variables demonstrate moderate changes as compared with their initial values.

Snapshots of an iso-surface of the *q*-criterion colored with pressure contours obtained for the baseline and optimized configurations at three time levels n = 48, 55, 63 are shown in Fig. 8. As in the previous test, the leading edge vortex generated by the wing with the optimized kinematic parameters is stronger than that obtained in the baseline case. Note, however, that the strengthening of the leading edge vortex mostly occurs due to the increase in the pitch and stroke amplitudes rather than their frequencies as in the foregoing test case. It should also be noted that the vortex size and intensity are lower than those obtained in the previous problem.

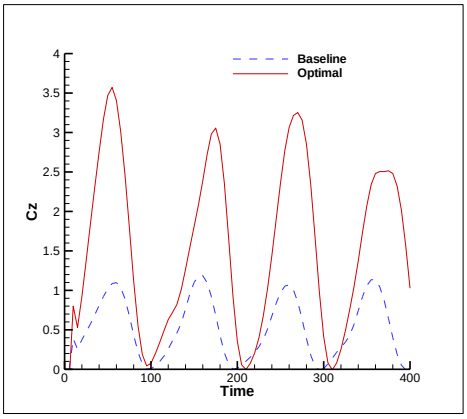

Figure 9: Baseline and optimal thrust profiles.

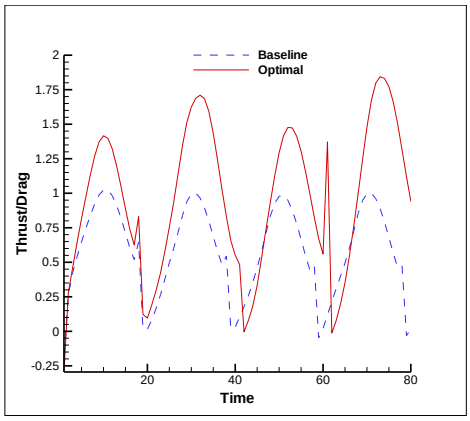

Figure 10: Propulsive efficiency before and after optimization for the 2nd test problem.

As follows from Fig. 9, the mean value of the thrust coefficient over the final 40 time steps has been increased by a factor of 2.9 after the optimization of the wing kinematics. Figure 10 shows the modified propulsive efficiency before and after optimization. The mean-stroke value of the propulsive efficiency computed with the penalized objective functional defined by Eq. (10) is about 65% higher than its baseline value. This improvement in the wing performance is achieved by imposing a proper constraint of the power required for the wing operation. It is expected that even higher performance gains are possible with including shape design variables into optimization, which would further expand the design space and open new avenues for optimization of flapping wing flows.

7 Conclusion

The kinematics of a hovering wing undergoing insect-based flapping motion has been optimized by using the time-dependent adjoint-based methodology developed in [13, 14]. In contrast to other optimization techniques, the adjoint formulation allows to compute the sensitivity derivatives with respect to all design variables at a cost comparable to that of a single flow solution. Two optimization problems with different objective functionals have been considered. For each test case, 15 kinematic parameters including amplitudes and frequencies of three angles defining the wing position as well as the coordinates of the wing root are used as design variables. The objective of the first test problem is to maximize the wing thrust. In the course of optimization, the mean value of the thrust coefficient has been increased by a factor of 5.5 as compared with its baseline value. The flapping frequency has been significantly increased by the optimizer, thus leading to increase in the wing drag. As a result, no appreciable improvements in the wing propulsive efficiency as compared with that of the baseline configuration have been obtained. To maximize the wing thrust while minimizing the drag and consequently the power required for the wing operation, we penalized the objective functional used in

the first test problem such that the functional rapidly increases if the aerodynamic force components in the wing stroke plane significantly deviate from zero. For this optimization problem, the optimizer has increased not only the stroke-averaged wing thrust by a factor 2.9, but also the wing propulsive efficiency by 65% as compared with that of the baseline configuration. These results indicate that the time-dependent adjoint-based methodology developed in [13, 14] is capable of significantly improving the flapping wing performance while satisfying the imposed constraints and can be used a powerful tool for optimization of flapping wing flows.

8 Acknowledgements

The authors would like to thank Eric Nielsen of NASA Langley Research Center for many helpful discussions pertaining to the current work and acknowledge the support from Army Research Laboratory through grant W911NF-06-R-006.

References

[1] M. F. Platzer and K.D. Jones, "Flapping-wing Aerodynamics: Progress and Challenges," AIAA Journal, Vol. 46(9), pp. 2136-2149, 2008.

[2] W. Shyy, H. Aono, K Chimakurthi, P Trizila, C K Kang, C E S Cesnik, H Liu, "Recent progress in flapping wing aerodynamics and aeroelasticity," Progress in Aerospace Sciences, Vol. 46(7), pp. 284-327, 2010.

[3] P. -O. Persson, D. J. Willis and J. Peraire, The Numerical Simulation of Flapping Wings at Low Reynolds Numbers, AIAA Paper 2010-724, 2010.

[4] R. Malhan, V.K. Lakshminarayan, J. Baeder, I. Chopra, "CFD investigation of aerodynamics of rigid flapping wings for MAV applications: Methodology validation ", Pros. of the AHS Specialists Conference, Jan 25-27, Tempe, 2011.

[5] M. Jones and N. Yamaleev, "The effect of a gust on the flapping wing performance," AIAA 2012-1080, 2012.

[6] Hamdaoui, J.-B. Mouret, S. Doncieux and P. Sagaut, Optimization of Kinematics for Birds and UAVs using Evolutionary Algorithms, Proceedings of the World Academy of Science, Engineering and Technology, Vol. 30, July 2008.

[7] K. Ito, "Optimization of Flapping Wing Motion," ICAS 2002 Congress, 2002.

[8] M. Milano, M. Gharib, "Uncovering the physics of flapping flat plates with artificial evolution," J. Fluid Mech., Vol. 534, pp. 403-409, 2005.

[9] M. Culbreth, Y. Allaneau, A. Jameson, "High-Fidelity Optimization of Flapping Airfoils and Wings," AIAA P. 2011-3521, 2011.

[10] H. Tuncer and M. Kaya, Optimization of Flapping Airfoils for Maximum Thrust and propulsive Efficiency, Acta Polytechnica, Vol. 44, No. 1, 2004.

[11] B. K. Stanford and P. S. Beran, "Cost reduction techniques for the design of non-linear flapping wing structures," Int. J. Numer. Meth. Eng. Vol. 88, pp. 533-555, 2011.

[12] E. Nielsen, B. Diskin, "Discrete adjoint-based design for unsteady turbulent flows on dynamic overset unstructured grids," AIAA P. 2012-0554, 2012.

[13] N. Yamaleev, B. Diskin, E. Nielsen, "Adjoint-based methodology for time-dependent optimization," AIAA Paper 2008-5857, 2008.

[14] E. Nielsen, B. Diskin, N. Yamaleev, "Discrete adjoint-based design optimization of unsteady turbulent flows on dynamic unstructured grids," AIAA J., Vol. 48, No.6, pp. 1195-1206, 2010.

[15] R. T. Biedron and J. L. Thomas, "Recent Enhancements to the FUN3D Flow Solver for Moving Mesh Applications," AIAA 2009-1360, 2009.

[16] Anderson,W. K., and Bonhaus, D. L., "An Implicit Upwind Algorithm for Computing Turbulent Flows on Unstructured Grids," Computers & Fluids, Vol. 23, No. 1, 1994.

[17] FUN3D official web site: http://fun3d.larc.nasa.gov

[18] L. Kaufman and D. Gay, "PORT Library: Optimization and Mathematical Programming – User's Manual," Bell Laboratories, 1997.